UNNS Substrate Research Program | Working Manuscript | 2026

Admissible Boundary Routing:

Structural Classification of Terminal Approach, Finite Bounce, and Cosmological Recession

Cosmological Boundary Routing Pilot Corpus

Instruments: STRUC-PERC-I v2.5.0 · STRUC-I v1.0.4 · Bridge v1.1 · α-Deformation v2.0/v2.2

UNNS Substrate Research Program

`unns.tech`

Companion manuscripts: Stellar Boundary Dynamics I · The Margin-Confinement Law · Percolative Realizability Principle · Admissible Cluster Geometry

Corpus: 3 synthetic model trajectories · 4 structural analysis layers · Planck 2018 observational anchor · Pilot scale

Abstract

The physical description of cosmological singularity removal operates at two levels: the equation level (whether the dynamics contain a divergence) and the observable level (whether density and curvature remain bounded). Neither level characterizes the topology of structural continuation through the critical regime. This manuscript introduces a third level, the route-topology level, and applies it to three matched cosmological model trajectories processed through the UNNS boundary-routing framework.

The three trajectories are: Dataset A (classical Friedmann contraction toward $a \to 10^{-8}$), Dataset B (effective Loop Quantum Cosmology bounce), and Dataset C (Planck 2018-anchored ΛCDM expansion). All three canonical direct ladder encodings

return FULL-percolation with zero HARD, GIANT, or TAIL outcomes and $A_\kappa = 1$ throughout. Dataset B carries higher structural pressure ($\bar{\rho} = 0.306$ versus $\bar{\rho} \approx 0.042$ for A and C) and a delayed connectivity threshold ($\kappa_{\text{conn}} = 0.100$, approximately $7.5\times$ A and C) while remaining admissible. The full Dataset B path achieves 98.83% α-admissibility persistence; all detected instability is confined to symmetric near-bounce shells, with all tested α-deformations of the two bounce-crossing intervals remaining admissible.

The principal result is the identification of three distinct *route-topology classes* via an orientation-sensitive bridge: terminal boundary approach (A, route coordinate $-1 \to 0$); finite turning-locus routing (B, $-1 \to 0 \to +1$); boundary recession (C, $0 \to +1$). These classes are computationally distinguishable within this controlled pilot corpus; magnitude-only representations erase the distinction between A and C, which is recovered only by signed orientation encoding.

The manuscript's thesis is: *singularity avoidance is not fully characterized by bounded curvature or a nonzero minimum scale factor alone. Structurally, it is the replacement of terminal route topology by admissible turning topology.* This extends the boundary-routing framework of Stellar Boundary Dynamics I, which identified branching routing as a first morphology. The cosmological corpus contributes a second: turning-locus routing. All results are scoped to the pilot corpus.

Contents

1 Introduction

1.1 Three levels of description for singularity removal

The standard cosmological treatment of singularity removal operates at two distinct language levels that are often conflated.

The *equation level* asks whether the dynamical equations contain a divergent point. Classical Friedmann dynamics do: as $a \to 0$, density and curvature grow without bound. Effective Loop Quantum Cosmology (LQC) removes this by introducing a correction term that caps the density at a critical value ρ_c, replacing the singular point with a finite bounce at $a_{\min} > 0$.

The *observable level* asks whether physical quantities remain bounded. In the LQC model, density and curvature are bounded by construction. This is the usual claim of singularity avoidance: bounded density and bounded curvature replace the classical divergence.

These two levels, however, do not characterize the *topology of structural continuation through the critical regime*. A trajectory can have bounded curvature while still approaching a terminal structural limit; conversely, a trajectory can cross a provisional zero of a margin component while remaining tested-admissible and continuing without structural destruction.

This manuscript introduces a third level: the *route-topology level*. It asks not whether dynamics diverge and not whether observables blow up, but what structural route class the trajectory occupies as it passes through or approaches the critical regime. Three distinct route classes are identified and formally defined: terminal approach, finite turning-locus routing, and boundary recession.

1.2 The structural argument

The argument runs in eight steps.

1. Classical Friedmann contraction approaches a terminal singular limit. The scale factor decreases, density and curvature diverge, and the selected classical trajectory chart contains no continuation beyond the terminal cutoff. This is the control case.

2. Effective LQC replaces the singular limit with a finite bounce at $a_{\min} > 0$. The usual claim is that this avoids the singularity because curvature and density remain bounded. We ask a more structural question: what is the route class?

3. We introduce orientation-sensitive structural encoding and define a shared route coordinate $s \in [-1, +1]$ based on cumulative $|\Delta \ln a|$. Under magnitude-only representation, classical contraction (A) and classical expansion (C) are degenerate because route orientation is erased. Dataset B remains distinguishable through its broader gap hierarchy, elevated connectivity threshold ($\kappa_{\text{conn}} = 0.100$ versus 0.013), structural pressure, and α-vector. However, B's finite reversal topology is visible only under signed-flow encoding.

4. We construct three matched synthetic trajectory datasets (A, B, C), process them through four structural analysis layers (STRUC-PERC-I, STRUC-I, α-deformation, Bridge v1.1), and extract route-topology signatures.

5. All three canonical direct ladder encodings return FULL-percolation. Admissibility is preserved in all three. But Dataset B occupies a structurally higher-pressure regime, and the orientation-sensitive bridge separates all three trajectories into distinct route classes.

6. The effective LQC path reaches a finite turning locus ($H = 0$, $\rho = \rho_c$) at which all tested α-deformations of the two bounce-crossing intervals are admissible. Its direct post-bounce ladder separately maintains $A_\kappa = 1$ throughout the tested STRUC-I range. The route reverses orientation and continues. This is finite turning-locus routing.

7. The classical Friedmann trajectory approaches a terminal cutoff with no continuation: terminal boundary approach. The Planck expansion recedes from the early critical regime: boundary recession. All three classes are computationally distinguishable.

8. The key theoretical result is: at the LQC bounce, the provisional margin component $1 - \rho/\rho_c = 0$. Yet the trajectory is tested-admissible at the turning locus under every applied deformation. This demonstrates that a structural boundary coordinate can mark admissible route reversal rather than structural destruction. The discriminating test is not the coordinate value but the route class.

1.3 Main results

The cosmological boundary routing pilot corpus produces five principal results.

(i) **Direct percolation.** All three canonical encodings return FULL with zero violations. $\kappa_{\text{conn}}(\text{B})/\kappa_{\text{conn}}(\text{A}, \text{C}) \approx 7.50$.

(ii) **Structural pressure.** Dataset B is Weak Persistence ($\bar{\rho} = 0.306$); A and C are Stable Structure ($\bar{\rho} \approx 0.042$). All three maintain $A_\kappa = 1$.

(iii) **Alpha-deformation.** Dataset B achieves 98.83% α-admissibility persistence. All 982 unstable rows are confined to symmetric near-bounce shells; all tested deformations of the two bounce-crossing intervals admissible.

(iv) **Route-topology classification.** The orientation-sensitive bridge assigns three distinct route classes. Magnitude-only encoding cannot produce this distinction.

(v) **Turning-shell localization.** Deformation sensitivity concentrates symmetrically around the bounce while the exact crossing remains tested-admissible under all applied α-deformations, motivating the Turning-Locus Shielding Hypothesis 9.1.

1.4 Relation to prior manuscripts

This work extends three prior UNNS manuscripts.

The **Stellar Boundary Dynamics I** corpus [5] established *branching routing*: catastrophic stellar collapse preserves FULL-percolation in all post-collapse observables while routing structure into non-equivalent downstream regimes. Its key theorem is that $\text{FULL}(\text{A}) \wedge \text{FULL}(\text{B}) \wedge \text{FULL}(\text{C})$ does not imply $\text{A} \approx_{\text{bridge}} \text{B} \approx_{\text{bridge}} \text{C}$.

The present corpus establishes a complementary morphology, *turning-locus routing*, with an analogous formal result replacing bridge equivalence by route-topology equivalence. Together they provide the first two members of a broader Boundary Routing taxonomy (Section 13).

The **Margin-Confinement Law** [3] establishes that identity-preserving physical trajectories cannot persistently cross into HARD fragmentation. The cosmological result refines this: a finite critical locus associated with the provisional boundary coordinate can act not merely as a terminal barrier but as a turning structure for admissible flow (Section 14).

The **Admissible Cluster Geometry** [4] framework organizes $\mathcal{M}_{\mathrm{adm}}$ into basins and corridors. The cosmological experiment adds a new internal-topology object: the *turning corridor* (Section 10).

1.5 Scope and organization

This is a pilot-corpus manuscript. Datasets A and B are synthetic model constructions; Dataset C is anchored to Planck 2018 parameters [17] but is likewise a trajectory integration. The route-topology classification is computationally established within the selected models and conventions. Formal results are scoped to the pilot corpus; conjectures are proposed as general principles requiring replication.

Sections 2–3 develop the theoretical framework. Sections 4–8 present the data, methods, and results. Section 9 states the formal layer. Sections 10–17 develop the turning-corridor interpretation, comparison with standard bounce cosmology, cross-model taxonomy, relation to prior UNNS work, robustness criteria, perturbation implications, and the observational pipeline. Sections 16–18 address robustness, observational implications, and limitations.

2 Theoretical Background

2.1 Admissibility, percolation, and structural pressure

The Universal Structural Law (USL) [1] bounds inversion pressure by vulnerability capacity:

$$\mathrm{inv}(P_\varepsilon; L) \;\le\; \nu(V_\varepsilon(L)). \tag{1}$$

A ladder L is *admissible* if (1) holds. The STRUC-PERC-I instrument [2] sweeps κ-connectivity thresholds and returns a four-tier verdict: FULL (GR = 1.000, zero isolated nodes), GIANT (GR $\geq$ 0.95), TAIL, or HARD. The STRUC-I instrument records admissibility metric $A_\kappa \in \{0, 1\}$ and structural pressure $\rho \in [0, 1]$ at each tested scale. The α-deformation operator applies multiplicative deformations $\alpha \in [0.50, 1.50]$ over a 21-point grid and returns a five-dimensional structural vector $\mathbf{v} = (\overline{\mathrm{GR}}, \sigma^2_{\mathrm{GR}}, \alpha_{\mathrm{aniso}}, \alpha_{\mathrm{persist}}, r_{\mathrm{onset}})$.

2.2 Prior vector bridge geometry

For multi-dataset comparisons, each object is embedded as a seven-feature structural vector derived from α-deformation outputs. The *vector bridge distance* between phases X and Y is

$$d(X, Y) = \|\bar{\mathbf{v}}(X) - \bar{\mathbf{v}}(Y)\|_2. \tag{2}$$

For the stellar corpus, the ABC bridge uses centroid-to-centroid distances in unified normalization space and derives the global routing geometry from equation (2).

The decisive cosmological result, however, does not come from equation (2). It comes from the orientation-sensitive Bridge v1.1, which constructs signed route profiles and a shared route coordinate rather than centroid distances. Section 8 describes Bridge v1.1 explicitly. The two bridge methods are distinct: the vector bridge measures structural positions in normalized feature space, while Bridge v1.1 measures route orientation and signed flow topology. Route-class assignments in this manuscript rely entirely on Bridge v1.1.

2.3 Motivation for a route-topology layer

The PRP framework characterizes connectivity within a single representation. But two trajectories with identical κ_{conn}, GR, and A_κ can differ fundamentally in whether the trajectory approaches a structural boundary or recedes from it. Sorted-magnitude ladders erase this information. Route topology is the additional structural coordinate needed to distinguish terminal, turning, and recession behavior.

3 Formal Route-Topology Framework

3.1 Orientation-sensitive structural encoding

Let $\mathcal{X}$ denote the ambient structural state space and let $\Gamma : [s_-, s_+] \to \mathcal{X}$ be an orientation-sensitive structural representation of a physical trajectory, parametrized by route coordinate $s \in [-1, +1]$. Where the UNNS admissibility criteria hold, $\Gamma(s) \in \mathcal{M}_{\text{adm}}$; this inclusion is one of the properties the analysis tests, not a prior assumption.

For single-branch trajectories (Datasets A and C), the route coordinate is constructed from cumulative $|\Delta \ln a|$:

$$s(t) = s_{\min} + \frac{\int_{t_0}^{t} |H(t')|dt'}{\int_{t_0}^{t_f} |H(t')|dt'}(s_{\max} - s_{\min}). \tag{3}$$

For turning routes (Dataset B), the coordinate is defined *piecewise*: the contraction arc maps the contraction branch to $s \in [-1, 0]$ and the expansion arc maps the expansion branch to $s \in [0, +1]$, with the bounce placed at $s = 0$ by construction. This piecewise definition remains valid for asymmetric bounces in which the two branch arc lengths differ.

Signed normalized flows are defined channel-wise as

$$f_i = \frac{\Delta_i}{\text{Q}_{90}(|\Delta_i|) + |\Delta_i|}, \qquad |f_i| \leq 1, \tag{4}$$

where Q_{90} is the 90th percentile of absolute increments, computed per dataset. The channels are: $\Delta \ln a$, H, physical density, curvature proxy, and provisional margin.

3.2 Route-topology classes

Definition 3.1 (Represented Terminal Approach)**.** A route Γ parametrized on $[-1, 0]$ is a *represented terminal approach at* $s = 0$ if: (i) the phase-mean normalized flow satisfies $\langle f_{\Delta \ln a} \rangle < 0$, so the net orientation points toward the route-zero locus; (ii) no continuation

is included in the selected chart beyond $s = 0$. The terminal designation refers to the represented route, not to the intrinsic nature of the underlying physical solution.

Definition 3.2 (Finite Turning-Locus Route)**.** A route Γ parametrized on $[-1, +1]$ contains a *finite turning locus at* $s = 0$ if:

(i) $\Gamma(0)$ is finite and all tested α-deformations of the exact turning-locus intervals are admissible: $A_\alpha(s = 0, \alpha_j) = 1$ for every tested α_j;

(ii) the scale factor orientation reverses: $\dot{a} < 0 \;\to\; \dot{a} = 0 \;\to\; \dot{a} > 0$;

(iii) the post-turning empirical phase-sign vector approximately reverses: $\bar{\mathbf{\Sigma}}_{P,\text{post}} \approx -\bar{\mathbf{\Sigma}}_{P,\text{pre}}$ for orientation-sensitive channels (Definition 3.5);

(iv) the route continues beyond $s = 0$ with reversed phase-mean signed flows, remaining in $\mathcal{X}$ with the tested region in $\mathcal{M}_{\text{adm}}$.

Definition 3.3 (Boundary Recession Route)**.** A route Γ parametrized on $[0, +1]$ is a *boundary recession route* if the phase-mean normalized flows satisfy $\langle f_{\Delta \ln a} \rangle > 0$ and $\langle f_m \rangle > 0$, so the net orientation moves away from the early boundary reference and the provisional margin tends to increase.

Definition 3.4 (Admissible Boundary Routing)**.** A physical trajectory exhibits *admissible boundary routing* when the exact turning-locus intervals remain admissible under all tested full-path α-deformations, the associated direct branch encoding remains admissible across its STRUC-I and STRUC-PERC-I range, and the route continues into a distinct branch without entering a terminal or non-realizable state.

3.3 The route-topology invariant: phase-sign vector

A pointwise sign field is $\mathbf{\Sigma}(s) = (\text{sgn} f_{\Delta \ln a}(s), \text{sgn} f_\rho(s), \text{sgn} f_{\mathcal{K}}(s), \text{sgn} f_m(s))$, which varies interval-by-interval. Because individual intervals may fluctuate, the empirically reliable object for route classification is the *empirical phase-sign vector*:

Definition 3.5 (Empirical Phase-Sign Vector)**.** For a route phase P (a contiguous set of intervals), the empirical phase-sign vector is

$$\bar{\mathbf{\Sigma}}_P \;=\; \Big(\text{sgn}\langle f_{\Delta \ln a}\rangle_P,\; \text{sgn}\langle f_\rho\rangle_P,\; \text{sgn}\langle f_{\mathcal{K}}\rangle_P,\; \text{sgn}\langle f_m\rangle_P\Big), \tag{5}$$

where $\langle \cdot \rangle_P$ denotes the phase-mean normalized flow.

The phase-mean object is what Tables 7–8 and the formal results (Propositions 9.1–9.2, Proposition 9.3) actually use. In the pilot corpus:

$$\bar{\mathbf{\Sigma}}_A = (-, +, +, -), \qquad \bar{\mathbf{\Sigma}}_C = (+, -, -, +),$$
$$\bar{\mathbf{\Sigma}}_{B,\text{pre}} = (-, +, \approx\!0, -), \qquad \bar{\mathbf{\Sigma}}_{B,\text{post}} = (+, -, \approx\!0, +).$$

The reversal condition $\bar{\mathbf{\Sigma}}_{B,\text{post}} \approx -\bar{\mathbf{\Sigma}}_{B,\text{pre}}$ holds for orientation-sensitive channels. The curvature channel is near-zero for Dataset B because the effective LQC correction redistributes the near-bounce curvature signal symmetrically. The empirical phase-sign vector defines a reproducible route classifier applicable to any bounce model processed through Bridge v1.1.

3.4 Boundary, turning locus, and inadmissible exterior

A structural boundary coordinate can mark two qualitatively different geometric events.

Definition 3.6 (Terminal Obstruction)**.** A structural route exhibits *terminal obstruction* in the selected chart when it approaches a represented critical reference locus and no continuation is included beyond that locus. Whether the reference locus coincides with $\partial\mathcal{M}_{\text{adm}}$ requires a canonical boundary metric and is not assumed here.

Definition 3.7 (Admissible Route Reversal)**.** A structural boundary coordinate marks *admissible route reversal* at $s = 0$ if: (i) $\Gamma(0)$ lies in the tested admissible region in the operational sense that all tested α-deformations assigned to the exact turning-locus intervals remain admissible, and the direct post-bounce encoding separately maintains $A_\kappa = 1$; (ii) $\bar{\mathbf{\Sigma}}_{P,\text{post}} \approx -\bar{\mathbf{\Sigma}}_{P,\text{pre}}$ for orientation-sensitive channels. The trajectory has reached a finite locus, reversed phase-mean orientation, and continues in the tested admissible region.

The discriminating test is not the value of any single coordinate (which may reach zero in both cases) but the route-topology class. In the cosmological setting, the provisional margin component $1 - \rho/\rho_{\text{c}} = 0$ at the LQC bounce. The route-topology analysis shows it marks an admissible route-reversal coordinate: the trajectory lies in the tested admissible region, the empirical phase-sign vector reverses, and the route continues.

Remark 3.1. Neither terminal obstruction nor admissible route reversal has been shown to require entry into the inadmissible exterior $\mathcal{M}^c_{\text{adm}}$. The terminal approach ends at the represented route-zero locus; turning routing continues through its finite route-zero locus. Their final geometric relationship to $\partial\mathcal{M}_{\text{adm}}$ remains open (Open Problem 14.1).

3.5 Three structural axes: admissibility, connectivity, depth

A key theoretical distinction of this corpus is that three structural axes must be kept separate.

Definition 3.8 (Structural Depth)**.** A FULL-percolating trajectory is *structurally deep* if $\bar{\rho} < \bar{\rho}_{\text{stable}}$ (Stable Structure) and *structurally shallow* if $\bar{\rho} \geq \bar{\rho}_{\text{stable}}$ (Weak Persistence). Both are admissible; structural depth is the operational pressure-based classification supplied by STRUC-I. Higher mean pressure indicates shallower persistence under that classifier, but is not yet identified with canonical metric distance to the admissibility boundary.

The three axes are:

- *Admissibility*: does $A_\kappa = 1$ hold? (All three datasets: yes.)
- *Connectivity*: at what κ_{conn} does the giant component form? (A,C: 0.01334; B: 0.10000.)
- *Structural depth*: how high is $\bar{\rho}$? (A,C: ≈ 0.042, Stable; B: 0.306, Weak.)

An admissible trajectory need not be deeply admissible. The implications are not reversible:

$$\text{FULL} \not\Rightarrow \text{low structural pressure}, \qquad A_\kappa = 1 \not\Rightarrow \text{small } \kappa_{\text{conn}}. \tag{6}$$

Dataset B is the clearest demonstration of this triaxial structure in the program: fully admissible, FULL-percolating, but shallow and with a delayed connectivity onset.

4 Dataset Construction

4.1 Three-trajectory design

The pilot corpus uses three matched synthetic trajectory datasets, summarized in Table 1. All three share Planck 2018 cosmological parameters [17]: $H_0 = 67.32\ \mathrm{km\,s^{-1}Mpc^{-1}}$, $\Omega_m = 0.3158$, $\Omega_\Lambda = 0.6842$, $\Omega_b h^2 = 0.02238$, $\Omega_c h^2 = 0.1201$.

Table 1: Pilot corpus dataset overview. Route coordinate: A covers $[-1, 0]$, B covers $[-1, +1]$, C covers $[0, +1]$.

Dataset	Physical role	Source	Rows	Route coord.
A – Classical Friedmann	Contraction toward terminal cutoff $a = 10^{-8}$	Synthetic; Planck 2018; $H < 0$	4001	$-1 \to 0$
B – Effective LQC	Contraction $\to$ bounce ($H = 0$) $\to$ expansion	Synthetic; eff. LQC v2.2; $\rho_c = 0.41\rho_{\mathrm{Pl}}$	4001	$-1 \to 0 \to +1$
C – Planck ΛCDM	Planck-compatible expansion	Planck 2018 best-fit	4001	$0 \to +1$

4.2 Dataset A: classical Friedmann contraction

Dataset A integrates the Friedmann equation $H^2 = H_0^2(\Omega_m a^{-3} + \Omega_\Lambda)$ backward with $H < 0$ from $a = 1$ to $a = 10^{-8}$ over 4001 uniformly spaced steps in $\ln a$. The terminal cutoff is a computational limit, not the mathematical singularity; Dataset A is the controlled reference for terminal-approach topology.

4.3 Dataset B: effective LQC bounce

Dataset B uses the effective LQC equation [9]

$$H^2 = H_0^2\,\rho_{\mathrm{rel}}\left(1 - \frac{\rho_{\mathrm{rel}}}{\rho_{\mathrm{c,rel}}}\right), \tag{7}$$

where $\rho_{\mathrm{c,rel}} = 0.41\,\rho_{\mathrm{Pl}}/\rho_{\mathrm{crit},0}$. Equation (7) reproduces standard Friedmann dynamics at low density and produces a bounce at $\rho_{\mathrm{rel}} = \rho_{\mathrm{c,rel}}$ where $H = 0$. Key bounce diagnostics: $a_{\min} = 2.468 \times 10^{-32}$; $H|_{\mathrm{bounce}} = 0$ (exact); $\rho/\rho_c|_{\mathrm{bounce}} = 1$ (exact turning surface); branch time to $a = 1$: 13.799 Gyr (Planck reference: 13.797 Gyr, difference <0.01%).

The hybrid grid comprises 2000 contraction + 1 bounce + 2000 expansion rows (4001 total). The direct STRUC-PERC-I ladder uses the post-bounce expansion branch only (2000 rows), because $\ln|H|$ is undefined at $H = 0$. The full signed path (4001 rows) is analyzed under α-deformation and Bridge v1.1.

4.4 Dataset C: Planck-anchored expansion

Dataset C integrates the standard Friedmann equation forward from $a = 10^{-8}$ to $a = 1$ using Planck 2018 best-fit parameters, providing a Planck-anchored reference background for the post-boundary expansion regime.

4.5 Orientation-sensitive encoding requirement

Under sorted-magnitude ladder encoding, Datasets A and C produce identical structural vectors. Both use $\ln(|H|/H_0)$ sorted by magnitude; both have $n = 4001$, $\kappa_{\text{conn}} = 0.01334$, and $\alpha_{\text{persist}} = 0.99262$. Route orientation (contraction vs. expansion) is erased. Bridge v1.1 restores orientation by preserving the signed flow f_i of equation (4) for all five channels.

5 Physical Trajectories: Qualitative Structure

Figure 1 illustrates the qualitative structure of the three trajectories.

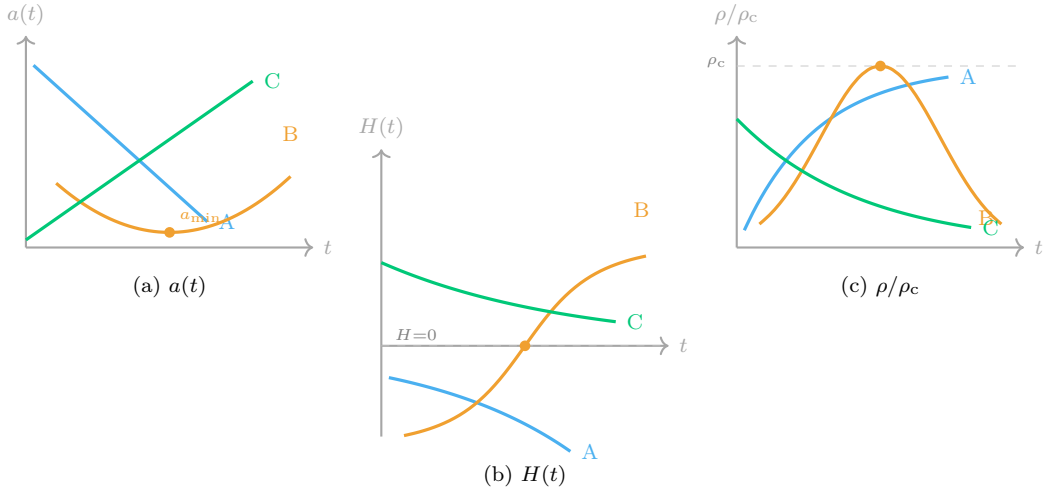

Figure 1: Schematic qualitative structure of the three trajectories. Panel (a): scale factor $a(t)$, showing contraction (A), bounce at $a_{\min}$ (B), and expansion (C). Panel (b): Hubble parameter $H(t)$, showing $H < 0$ (A), sign reversal at $H = 0$ (B, filled circle), and $H > 0$ decreasing (C). Panel (c): density ρ/ρ_c, showing growth toward divergence (A), peak at the critical density ρ_c (B, filled circle), and decay (C). These are schematic representations of the synthetic trajectory structure.

The key qualitative feature is at $t = t_{\text{bounce}}$ in Dataset B: H passes through zero while ρ/ρ_c peaks at 1. In effective LQC, this combination identifies the maximum-density turning point. The corresponding classical contracting trajectory has no finite reversal at this density and continues toward the $a \to 0$ singular regime. Here, the effective dynamics replace that continuation with a finite, tested-admissible turning locus. The structural analysis (Sections 6–8) quantifies what this means at the route-topology level.

6 Direct Connectivity and Structural Pressure

6.1 STRUC-PERC-I: 3/3 Full

Table 2 presents STRUC-PERC-I v2.5.0 results. All three canonical direct ladder encodings return Full with zero violations.

At $\kappa = 0.01$, Datasets A and C already have a dominant giant component (GR = 0.977, 77 components), reaching full connectivity at $\kappa_{\text{conn}} = 0.01334$. Dataset B's expansion ladder is substantially more fragmented (GR = 0.533, 22 components), requiring

Table 2: STRUC-PERC-I v2.5.0 results. $\mathrm{GR}_{\mathrm{init}}$: giant ratio at $\kappa = 0.01$; n_{comp}: components at $\kappa = 0.01$; $\mathrm{GR}_{\mathrm{final}}$: at κ_{conn}. B direct ladder: post-bounce expansion branch only.

Dataset	Verdict	κ_{conn}	$\mathrm{GR}_{\mathrm{init}}$	n_{comp}	$\mathrm{GR}_{\mathrm{final}}$	n
A – Classical Friedmann	FULL	0.01334	0.97675	77	1.000	4001
B – LQC (expansion)	FULL	0.10000	0.53277	22	1.000	2000
C – Planck ΛCDM	FULL	0.01334	0.97675	77	1.000	4001

$\kappa_{\mathrm{conn}} = 0.10000$. The connectivity-threshold ratio is $\kappa_{\mathrm{conn}}(\mathrm{B})/\kappa_{\mathrm{conn}}(\mathrm{A,C}) \approx 7.50$. Figure 2 illustrates this.

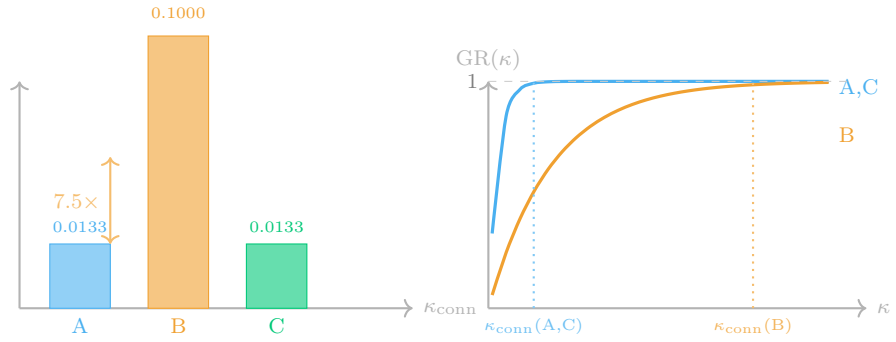

(a) κ_{conn} comparison (b) Schematic GR vs κ

Figure 2: Direct connectivity comparison. Panel (a): κ_{conn} values for A, B, C; B requires ≈7.5× larger threshold than A and C. Panel (b): schematic GR(κ) curves showing the delayed onset for Dataset B (LQC expansion encoding) relative to A and C. All three reach GR = 1.000 at their respective κ_{conn}.

The elevated κ_{conn} for Dataset B is not an admissibility violation. The selected post-bounce LQC expansion encoding carries a broader gap hierarchy than the matched classical encodings. This observation is consistent with, but does not by itself causally isolate, structural inheritance from the preceding bounce transition; the α-deformation analysis (Section 7) localizes behavior around the quantum-transition shell.

6.2 STRUC-I structural pressure

Table 3 presents STRUC-I v1.0.4 results. All three direct encodings maintain $A_\kappa = 1.000$ throughout the tested κ range; no direct ladder enters a non-realizable state. Dataset B occupies a substantially higher-pressure admissible regime.

Table 3: STRUC-I v1.0.4 results. B direct ladder: post-bounce expansion only. All three satisfy $A_\kappa = 1$ throughout.

Dataset	State	$\min A_\kappa$	$\bar{\rho}$	$\rho_{\max}$	$\rho_{\kappa=1}$
A – Classical Friedmann	Stable Structure	1.000	0.04157	0.290	0.290
B – LQC (expansion)	Weak Persistence	1.000	0.30605	0.636	0.451
C – Planck ΛCDM	Stable Structure	1.000	0.04163	0.291	0.291

The pressure ratio $\bar{\rho}(\mathrm{B})/\bar{\rho}(\mathrm{A,C}) \approx 7.4$. Dataset B is admissible ($A_\kappa = 1$) but operates under substantially higher deformation pressure. This elevated pressure is measured in the post-bounce LQC expansion ladder and reflects its broader sorted gap geometry.

Proposition 6.1 (Admissibility Does Not Determine Structural Depth)**.** *In the cosmological boundary routing pilot corpus,* FULL*-percolation and* $A_\kappa = 1$ *throughout are consistent with three distinct structural-depth regimes:*

$$\text{FULL(A)} \wedge \text{FULL(B)} \wedge \text{FULL(C)} \not\Rightarrow \bar{\rho}(\text{A}) \approx \bar{\rho}(\text{B}) \approx \bar{\rho}(\text{C}). \tag{8}$$

Specifically: A and C are Stable Structure ($\bar{\rho} \approx 0.042$*); B is Weak Persistence (*$\bar{\rho} = 0.306$*), a factor of* $\approx$7.4 *higher.*

7 Alpha-Deformation Geometry

7.1 Five-dimensional structural vectors

Table 4 presents the five-dimensional α-deformation vectors.

Table 4: α-deformation vectors. $\alpha \in [0.50, 1.50]$, 21-point grid, 84,000 total deformation rows. A and C are degenerate under magnitude-only encoding.

Dataset	$\overline{\text{GR}}$	σ^2_{GR}	α_{aniso}	α_{persist}	r_{onset}	Unstable/84 000
A – Classical Friedmann	0.24447	0.02229	0.17287	0.99262	0.45	620
B – Effective LQC	0.25963	0.04145	0.00117	0.98831	0.05	982
C – Planck ΛCDM	0.24447	0.02229	0.17287	0.99262	0.45	620

7.2 Instability localization and turning-shell structure

Table 5 reports the distribution of unstable rows within Dataset B's five structural regions.

Table 5: Dataset B α-instability by region. Near-bounce shells: $0.03 \leq \rho/\rho_c \leq 0.82$.

Region	Unstable rows	Fraction
Contraction outer	0	0.000
Contraction near-bounce shell	491	0.006
Bounce crossing (exact)	0	0.000
Expansion near-bounce shell	491	0.006
Expansion outer	0	0.000
Total	982	0.012

The pattern is striking: all tested α-deformations of the two bounce-crossing intervals are admissible, while 982 rows are confined symmetrically to the near-bounce shells (491 each side, onset radius $r_{\text{onset}} = 0.05$). Figure 3 illustrates this layered geometry.

Observation 7.1. The spatial pattern is consistent with a turning-locus shielding pattern: sensitivity peaks in the neighborhood of the turning locus while the locus itself remains protected. This pattern is the principal empirical motivation for Hypothesis 9.1.

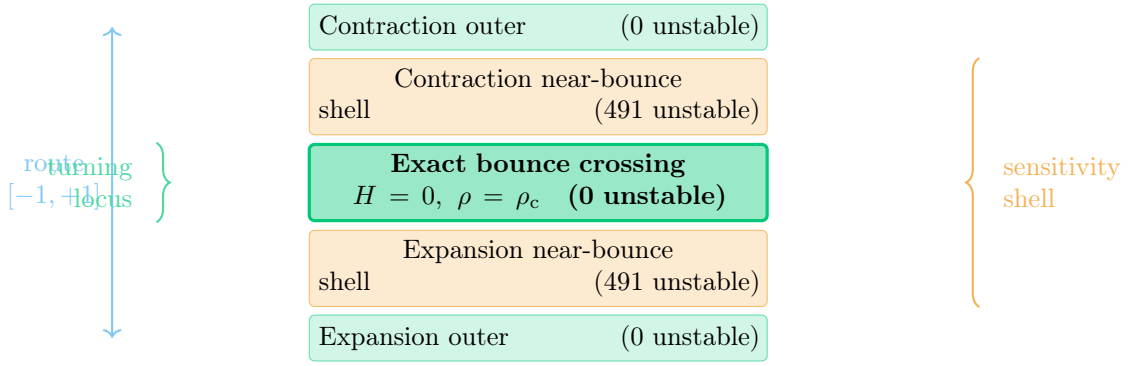

Figure 3: Turning-shell geometry of Dataset B. All tested α-deformations of the two bounce-crossing intervals remain admissible, with zero unstable rows at the exact crossing. All instability is confined to symmetric near-bounce shells (491 rows each side, $0.03 \leq \rho/\rho_c \leq 0.82$). Outer regions are fully stable. The route passes continuously through the center.

8 Orientation-Sensitive Bridge

8.1 Why magnitude-only geometry fails

Under sorted-magnitude ladder encoding, Datasets A and C are structurally degenerate: identical κ_{conn}, GR, A_κ, and α-vectors. Classical Friedmann contraction and Planck ΛCDM expansion are indistinguishable. This degeneracy is not a numerical coincidence. It reflects a general principle:

A representation can preserve scale geometry while erasing route topology.

8.2 Chart-completeness analysis

Table 6: Chart-completeness analysis. Each row lists what a given structural encoding preserves (and which question it can answer).

Chart	Connectivity	Branch ID	Orientation	A/C resolved	Notes
Sorted magnitude ladder	Yes	No	No	No	κ_{conn}, GR correct; route class erased
Full signed α path	Yes	Yes	Partial	No	magnitude degeneracy persists in $\mathbf{v}$
Bridge v1.1	Yes	Yes	Yes	Yes	signed flows recover $\bar{\mathbf{\Sigma}}_{P,A} \neq \bar{\mathbf{\Sigma}}_{P,C}$

Table 6 formalizes the encoding hierarchy. A scalar ladder is canonical for connectivity analysis; an orientation-sensitive chart is canonical for route-topology classification. Canonicality is question-dependent: the choice of representation must match the structural

question being asked. This is one of the clearest demonstrations in the UNNS program of the Representation-Driven Structure principle [7].

8.3 Bridge v1.1: signed-flow construction

Bridge v1.1 preserves five signed normalized flow channels (equation 4) and assigns a shared route coordinate $s \in [-1, +1]$: A covers $[-1, 0]$, B covers $[-1, +1]$, C covers $[0, +1]$. Tables 7–8 present results.

Table 7: Bridge v1.1 signed-flow summary. Full-path B means are near-zero due to pre/post-bounce cancellation; branch-resolved values (Table 8) are authoritative.

Dataset	Route class	Route coord.	$\overline{f}_{\Delta \ln a}$	$\overline{f}_{\rho}$	$\overline{f}_{m}$
A	Terminal approach	$-1 \to 0$	-0.500	$+0.463$	-0.093
B	Finite turning-locus	$-1 \to 0 \to +1$	≈ 0	≈ 0	≈ 0
C	Boundary recession	$0 \to +1$	$+0.500$	-0.463	$+0.093$

Table 8: Branch-resolved profile for Dataset B. Turning-surface H-flow mean $\approx 1.76 \times 10^{-4}$ (near-zero but not identically zero; $\overline{f}_{\Delta \ln a}$, $\overline{f}_{\rho}$, $\overline{f}_{m}$ are zero by exact branch symmetry).

Phase	Intervals	Route coord.	$\overline{f}_{\Delta \ln a}$	$\overline{f}_{\rho}$	$\overline{f}_{m}$
A terminal approach	4000	$-1 \to 0$	-0.500	$+0.463$	-0.093
B pre-bounce	1999	$-1 \to \approx 0$	-0.305	$+0.299$	-0.100
B turning surface	2	≈ 0	0	0	0
B post-bounce	1999	$\approx 0 \to +1$	$+0.305$	-0.299	$+0.100$
C boundary recession	4000	$0 \to +1$	$+0.500$	-0.463	$+0.093$

The reversal condition $\bar{\mathbf{\Sigma}}_{P,B,\text{post}} \approx -\bar{\mathbf{\Sigma}}_{P,B,\text{pre}}$ holds with $|\overline{f}_{\Delta \ln a}| = 0.305$ (both branches) and $|\overline{f}_{m}| = 0.100$ (both branches). This pre/post symmetry is the structural signature of route reversal through an admissible turning locus. Figure 4 visualizes the phase-mean flows.

8.4 Route topology diagram

Figure 5 illustrates the three route classes in the shared coordinate.

9 Formal Layer

9.1 Definitions

Definitions 3.1–3.7 were stated in Section 3. We add one more.

Definition 9.1 (Route-Topology Equivalence)**.** Two routes Γ_1, Γ_2 are *route-topology equivalent* ($\Gamma_1 \equiv_{\text{route}} \Gamma_2$) if their route classes agree and their empirical phase-sign vectors $\bar{\mathbf{\Sigma}}_P$ agree for all orientation-sensitive channels, under a consistent phase decomposition.

9.2 Propositions

Proposition 9.1 (Admissibility Does Not Determine Route Topology)**.** *In the cosmological boundary routing pilot corpus,* FULL*-percolation and near-full α-admissibility persistence*

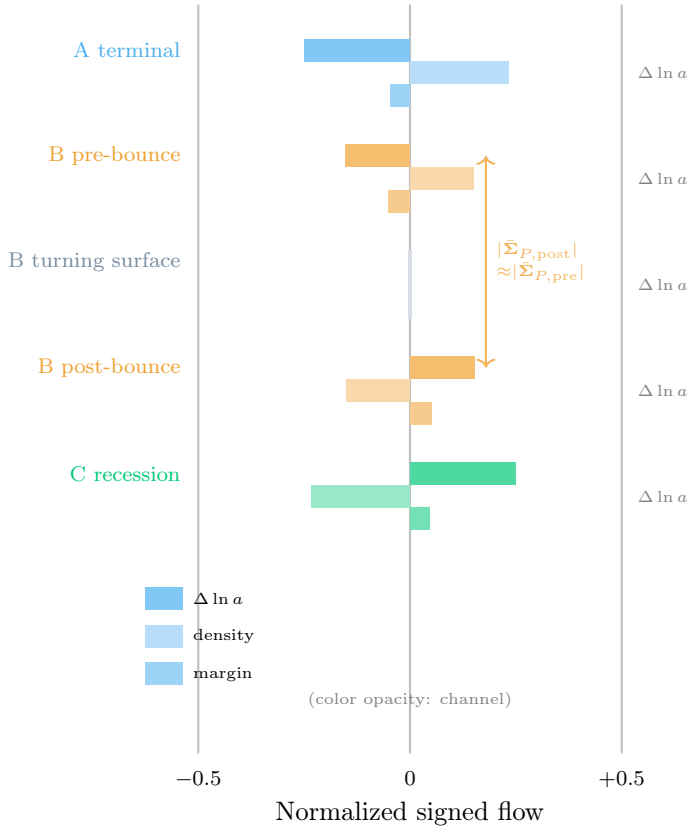

Figure 4: Branch-resolved phase-mean signed flows for all five route phases. Dark bars: $\Delta \ln a$ (scale factor orientation); medium bars: density flow; light bars: margin flow. Bars extend right for positive flows and left for negative. The pre-bounce and post-bounce branches of Dataset B exhibit near-perfect sign reversal ($\bar{\mathbf{\Sigma}}_{P,B,\text{post}} \approx -\bar{\mathbf{\Sigma}}_{P,B,\text{pre}}$), the structural signature of finite route reversal. Turning-surface flows are near-zero (gray).

are consistent with three mutually non-equivalent route classes:

$$\textsc{Full}(\text{A}) \wedge \textsc{Full}(\text{B}) \wedge \textsc{Full}(\text{C}) \;\not\Rightarrow\; \text{A} \equiv_{\text{route}} \text{B} \equiv_{\text{route}} \text{C}. \tag{9}$$

Proof. All three canonical direct ladders return FULL (Table 2). Bridge v1.1 assigns empirical phase-sign vectors $\bar{\mathbf{\Sigma}}_{P,A} = (-,+,+,-)$, $\bar{\mathbf{\Sigma}}_{P,C} = (+,-,-,+)$, $\bar{\mathbf{\Sigma}}_{P,B,\text{pre}} = (-,+,\approx\!0,-)$, $\bar{\mathbf{\Sigma}}_{P,B,\text{post}} = (+,-,\approx\!0,+)$. These are mutually non-equivalent (Tables 7–8). □

Proposition 9.2 (A and C Are Magnitude-Degenerate but Route-Distinct)**.** *Datasets A and C are degenerate under sorted-magnitude encoding (κ_{conn}, GR, A_κ, α-vectors all identical) and route-distinct under orientation-sensitive encoding ($\bar{\mathbf{\Sigma}}_{P,A} \neq \bar{\mathbf{\Sigma}}_{P,C}$; each phase-mean component reverses in sign).*

Proof. Degeneracy: Tables 2–4 give identical values for A and C. Distinction: Table 7 gives $\overline{f}_{\Delta \ln a}(\text{A}) = -0.500 \neq +0.500 = \overline{f}_{\Delta \ln a}(\text{C})$; density and margin flows also reverse. □

Remark 9.1. Propositions 6.1–9.2 jointly establish that three distinct structural axes are required: admissibility (Proposition 9.1), structural depth (Proposition 6.1), and route orientation (Proposition 9.2). None implies the others.

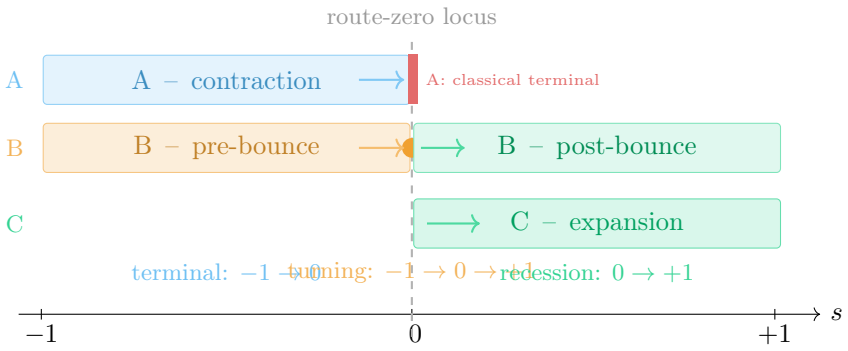

Figure 5: Route-topology diagram. Dataset A (blue): terminal approach, route terminates at $s = 0$ (red terminal wall). Dataset B (amber/green): finite turning-locus route, continuous through $s = 0$ (filled circle = bounce locus); arrows show route-coordinate progression. Dataset C (green): boundary recession from $s = 0$. The dashed line marks the shared route-zero locus, which has different structural meaning for each row: A reaches a terminal cutoff, B reaches the finite LQC bounce, C begins its Planck-compatible expansion.

9.3 Pilot-corpus verified result

Proposition 9.3 (Cosmological Boundary Routing—Pilot-Corpus Verified Result)**.** *In the cosmological boundary routing pilot corpus, the three analyzed trajectories satisfy:*

(i) All three canonical direct encodings return Full *with zero* Hard, Giant, *or* Tail *outcomes and* $A_\kappa = 1$ *throughout.*

(ii) The full Dataset B path achieves 98.83% α*-admissibility persistence; all 982 unstable rows are confined to symmetric near-bounce shells, with all tested* α*-deformations of the two bounce-crossing intervals remaining admissible.*

(iii) The orientation-sensitive Bridge v1.1 assigns three distinct route-topology classes on the basis of empirical phase-sign vectors: represented terminal approach (A), finite turning-locus routing (B), and boundary recession (C).

Within this processed pilot corpus, the effective LQC trajectory is structurally represented as finite admissible turning: it reaches a critical locus, all tested deformations of that locus are admissible, the empirical phase-sign vector reverses ($\bar{\boldsymbol{\Sigma}}_{B,\mathrm{post}} \approx -\bar{\boldsymbol{\Sigma}}_{B,\mathrm{pre}}$*), and the route continues without structural destruction. This result follows directly from the archived STRUC-PERC-I, STRUC-I,* α*-deformation, and Bridge v1.1 outputs.*

Proof. (i) Tables 2–3. (ii) Table 5; bounce-crossing regions: 2 intervals, 0 unstable. (iii) Tables 7–8; reversal: $|\langle f_{\Delta \ln a} \rangle| = 0.305$ (pre) $= 0.305$ (post), $|\langle f_m \rangle| = 0.100$ (both branches). □

Remark 9.2. The above result is scoped to the pilot corpus and one effective LQC construction. It is a derivable consequence of the measured computational outputs; generalization requires replication across additional bounce models, grid refinements, and normalization variants.

9.4 Conjectures and hypotheses

Conjecture 9.1 (Boundary Routing—Cosmological)**.** A non-singular cosmological model may exhibit admissible boundary routing (Definition 3.4) when its effective dynamics replace the terminal Friedmann limit with a finite turning locus. In such cases, the UNNS route class changes from terminal approach to finite turning-locus routing without structural destruction.

Hypothesis 9.1 (Turning-Locus Shielding)**.** A finite admissible turning locus may exhibit an apparent local shielding pattern: structural deformation sensitivity accumulates in a surrounding shell while the exact turning locus remains admissible under all tested deformations. *Evidence:* near-bounce shells contain 491 unstable rows each; all tested deformations of the two bounce-crossing intervals are admissible. This pattern has not yet been causally explained. The hypothesis would be falsified by instability at the exact locus, shell asymmetry, or disappearance under grid refinement or alternative normalization.

Conjecture 9.2 (Route-Sign Reversal as Turning Signature)**.** A trajectory is operationally identified as a finite turning-locus route when $\bar{\mathbf{\Sigma}}_{P,\mathrm{post}} \approx -\bar{\mathbf{\Sigma}}_{P,\mathrm{pre}}$ for orientation-sensitive channels, zero instability at the exact turning-locus intervals under all tested deformations, and continuous admissibility through the route change. This is a *sufficient* operational signature, not a necessary and sufficient characterization of every possible turning route: other bounce systems may satisfy alternative sufficient criteria. The classifier is applicable to other bounce models via Bridge v1.1.

10 The Turning Corridor in Admissible Cluster Geometry

The Admissible Cluster Geometry (ACG) framework [4] organizes $\mathcal{M}_{\mathrm{adm}}$ into: *admissible basins* (internally cohesive high-GR regions), *continuity corridors* (sparse connections between basins), *fragmentation barriers* (regions of elevated vulnerability), and *recoverable routes* (lifting paths from near-Hard to admissible).

The Stellar Boundary Dynamics corpus [5] added a dynamic layer: some basins are generated by boundary-routing events (collapse routes structure from one basin into separate post-boundary basins).

The cosmological corpus adds a qualitatively different internal-topology object:

Definition 10.1 (Turning Corridor)**.** A *turning corridor* is a connected route through the tested admissible region that narrows into a deformation-sensitive neighborhood around a finite turning locus, passes through a locus whose tested deformation rows remain admissible, and continues with reversed orientation.

Dataset B traces the following path: stable contraction region → narrowing near-bounce corridor (sensitivity shell, $r_{\mathrm{onset}} = 0.05$) → finite turning locus ($H = 0$, $\rho = \rho_{\mathrm{c}}$; all tested deformations admissible) → widening near-bounce corridor (symmetric expansion shell) → stable expansion region.

The exact turning locus behaves as a tested-admissible route-reversal point. Whether it lies in the mathematical interior of the final admissibility manifold remains open (Open Problem 14.1). The zero of $1 - \rho/\rho_{\mathrm{c}}$ locates the orientation reversal.

This turning-corridor object enriches the ACG picture:

- Ordinary continuity corridors: connect basins without reversal.
- Recovery corridors: lift fragmented representations into admissibility.
- **Turning corridors: connect two route orientations through a finite tested-admissible locus.**
- Branching junctions: route structure from one basin into multiple separated post-event basins (stellar case).

The turning corridor is the ACG realization of the cosmological bounce.

11 Comparison with Singularity-Avoidance Language

Three claims are often conflated in the singularity-avoidance literature:

(i) *Singularity removal*: the equations contain no divergent point.

(ii) *Bounded observables*: density, curvature, and related quantities remain finite.

(iii) *Admissible structural continuation*: all tested α-deformations of the exact turning-locus intervals are admissible, the direct post-bounce encoding maintains $A_\kappa = 1$, and the trajectory continues as a finite turning-locus route.

Effective LQC provides (i) by construction and (ii) by the critical-density bound. The UNNS analysis adds (iii).

The manuscript's original contribution relative to ordinary bounce cosmology is the following:

> *Bounded curvature alone does not define route topology. A non-singular model becomes an admissible boundary-routing model only when structural continuation through the critical locus is demonstrated: the trajectory must reach the turning locus finitely, preserve admissibility there, and continue with reversed orientation.*

The provisional margin component $1 - \rho/\rho_c$ equals zero at the bounce. This is not a failure: it marks the finite turning surface. The zero serves as a route-orientation coordinate; whether it signals terminal obstruction or admissible reversal is determined by route-topology class, not by the coordinate value itself (Definitions 3.6–3.7).

12 Relation to Standard Bounce Cosmology

12.1 Effective LQC and the UNNS structural layer

Dataset B implements the standard effective isotropic Loop Quantum Cosmology form [9]: the classical Friedmann equation is modified by a high-density correction,

$$H^2 = \frac{8\pi G}{3}\rho\left(1 - \frac{\rho}{\rho_c}\right), \tag{10}$$

where the low-density regime approaches the classical Friedmann solution while the contracting branch reaches $H = 0$ at the finite critical density ρ_c. The trajectory then continues onto an expanding branch. This mechanism is not introduced by the present

manuscript. Effective LQC already interprets it as quantum-geometric singularity resolution and has an extensive literature on bounded density, bounded curvature, geodesic extension of effective spacetime, anisotropic models, perturbation generation, and possible observational consequences [11, 10].

The UNNS analysis therefore operates as a *complementary classification layer*: standard effective LQC supplies the dynamical trajectory; UNNS assigns that trajectory a route-topology class and compares it with terminal classical contraction and boundary recession. The two frameworks address distinct questions, summarized in Table 9.

Table 9: Complementarity between standard effective LQC and UNNS Cosmological Boundary Routing.

Standard effective LQC	UNNS Cosmological Boundary Routing
What modification removes the classical divergence?	What structural route replaces terminal evolution?
Are density, curvature, and expansion quantities bounded?	Is the critical locus terminal, turning, branching, or receding?
Does the effective spacetime continue through the bounce?	What signed structural signature characterizes that continuation?
What perturbations and observables follow from the bounce?	Which admissibility, pressure, connectivity, and route class does the model occupy?

The UNNS route-topology layer adds four structural objects not normally used in standard LQC description:

(i) a shared, orientation-sensitive route coordinate;

(ii) empirical phase-sign vectors $\bar{\boldsymbol{\Sigma}}_P$ (Definition 3.5);

(iii) signed normalized structural-flow profiles;

(iv) a distinction between terminal obstruction and admissible route reversal (Definitions 3.6–3.7).

With these objects, the effective LQC bounce is represented not only as bounded evolution but as a continuous route whose pre- and post-bounce phase-sign vectors approximately reverse: $\bar{\boldsymbol{\Sigma}}_{P,B,\mathrm{post}} \approx -\bar{\boldsymbol{\Sigma}}_{P,B,\mathrm{pre}}$. The route-class assignments for the pilot corpus are:

$$\begin{aligned} &\text{classical contraction} &&\longrightarrow \text{ represented terminal approach},\\ &\text{effective LQC bounce} &&\longrightarrow \text{ finite turning-locus routing},\\ &\text{Planck-anchored expansion} &&\longrightarrow \text{ boundary recession}. \end{aligned} \tag{11}$$

The present result is restricted to effective background dynamics. It does not reproduce the full polymer-quantized theory, establish geodesic completeness independently, or test bounce-generated perturbations against observational likelihoods. The statement that all tested α-deformations of the two bounce-crossing intervals remain admissible is an operational result of the pilot corpus; it is not equivalent to a proof of geodesic completeness and should not be conflated with one. All singularity-resolution and geodesic-completeness claims in the LQC literature belong to that literature.

12.2 Mapping alternative models to route-topology classes

The route-topology framework is not tied to effective LQC. It supplies an operational language for comparing models whose microscopic mechanisms differ.

Ekpyrotic and cyclic models. Ekpyrotic cosmologies [16] contain a slow contracting phase followed by a nonsingular bounce and expansion. Such models are candidates for finite turning-locus routing when they satisfy $\dot{a} < 0 \to \dot{a} = 0 \to \dot{a} > 0$ with finite observables, tested admissibility at the transition, and post-transition continuation. The UNNS signature need not be symmetric: different matter content before and after the bounce may produce $|\bar{\mathbf{\Sigma}}_{P,\mathrm{pre}}| \neq |\bar{\mathbf{\Sigma}}_{P,\mathrm{post}}|$ even when their orientation-sensitive components reverse sign. Cyclic models would produce repeated turning loci and therefore a sequence of route reversals. Claims concerning anisotropy suppression or scale-invariant perturbations depend on the selected fields, potentials, and perturbation mechanism and must be tested model by model; they are not generic consequences of a nonsingular bounce.

Matter-bounce models. Matter-bounce constructions [15] begin with a matter-dominated contracting phase and introduce a nonsingular transition into expansion. Their expected route class is finite turning-locus routing. Their structural-pressure ($\bar{\rho}$) and onset-radius (r_{onset}) need not match effective LQC. A comparative test should determine whether the exact turning locus remains admissible, a surrounding sensitivity shell is present, and pre/post phase-sign vectors reverse.

Modified-gravity and higher-derivative bounces. Ghost-condensate, Galileon, $f(R)$, and string-inspired bounce models introduce different correction terms to generate a finite transition. Models with contraction followed by a finite bounce and expansion are candidates for turning-locus routing. Agreement in route class does not imply agreement in structural depth: two models could both be turning routes while occupying different connectivity (κ_{conn}) and pressure ($\bar{\rho}$) regimes.

Emergent and expanding-only models. Models that begin in a quasi-static or asymptotically past-eternal state and subsequently expand may contain no route reversal at all. Depending on early behavior, they may be classified as delayed boundary recession, a quasi-stationary corridor followed by recession, or a separate emergence class requiring extension of the present taxonomy. They should not automatically be assigned to the finite-turning category.

Conformal Cyclic Cosmology. Conformal Cyclic Cosmology [18] joins the asymptotic future of one aeon to the beginning of the next through conformal identification rather than a high-density contraction–bounce–expansion event. Its UNNS classification is therefore open. Possible interpretations include: cross-chart continuation across a conformal boundary; recession followed by representation renewal; or a higher-order cyclic junction structurally distinct from a finite turning locus. A classification would require a chart that retains the conformal rescaling and the transition between aeons; the present Bridge v1.1 criterion is not sufficient by itself. This motivates a proposed additional route morphology, *cross-chart continuation*, which is left as an open category in the taxonomy below.

12.3 Provisional cross-model taxonomy

Table 10 collects the expected route-topology assignments across major cosmological model families.

Table 10: Provisional route-topology taxonomy across cosmological model families. Realized: demonstrated in this pilot corpus. Prediction: expected from the model's dynamics under the UNNS criterion. Open: classification requires further chart construction or extension.

Model family	Expected route topology	Status
Classical singular Friedmann contraction	Represented terminal approach	Realized (Dataset A)
Effective LQC bounce	Finite turning-locus routing	Realized (Dataset B)
Planck-anchored expanding ΛCDM	Boundary recession	Realized (Dataset C)
Ekpyrotic nonsingular bounce	Turning-locus routing; possibly asymmetric pre/post	Prediction
Matter-bounce	Turning-locus routing	Prediction
Modified-gravity bounce	Turning-locus or model-dependent continuation	Prediction
Cyclic bounce models	Repeated turning-locus routing	Prediction
Emergent-universe models	Quasi-stationary corridor followed by recession	Open
Conformal Cyclic Cosmology	Cross-chart continuation or conformal junction	Open

The unifying structural question across all models is:

terminal obstruction | admissible turning | boundary recession | cross-chart continuation	(12)

This taxonomy makes models with very different microscopic dynamics comparable without treating them as physically equivalent. Route topology supplies a common structural language; connectivity, pressure, and deformation response retain the structural differences between individual models.

13 Relation to Stellar Boundary Dynamics

13.1 Two routing morphologies

The Stellar Boundary Dynamics I corpus [5] established *branching routing*: core-collapse supernovae preserve FULL-percolation in all observables while routing structure into non-equivalent downstream regimes (bridge class A-to-B contact with C branching; $d_{AB} = 0.401$, $d_{BC} = 1.287$, $d_{AC} = 1.365$). Identity-preserving continuation fails, but the post-boundary observables are each internally admissible and mutually non-equivalent.

The present corpus establishes a complementary morphology: *turning-locus routing*. Identity-preserving continuation is not broken; the trajectory reverses through a finite admissible locus and continues as continuous contraction and expansion branches joined at the finite turning locus.

Together they instantiate a general principle:

Admissibility-preserving boundary events can produce distinct topological signatures.

13.2 Unified boundary-routing morphology table

Table 11 contrasts the two realized morphologies and anticipates additional modes.

Table 11: Boundary-routing morphology taxonomy. The first two rows are established in the UNNS program; the remaining modes are anticipated or theoretically motivated.

Mode	Structural behavior	Route topology	Example
Terminal approach	Represented route ends at a limiting locus; no continuation included	$(-1 \to 0)$; $\langle f_{\Delta \ln a} \rangle < 0$	Classical Friedmann (A)
Turning-locus routing	Route reaches finite admissible locus, reverses orientation, continues	$(-1 \to 0 \to +1)$; phase-sign reversal	Effective LQC (B)
Boundary recession	Route moves away from early boundary regime	$(0 \to +1)$; $\langle f_m \rangle > 0$	Planck ΛCDM (C)
Branching routing	One event creates non-equiv. downstream regimes	A→B contact; C branches	Stellar Boundary Dynamics I
Recovery routing	Fragmented representation lifts into admissible form	Near-Hard → FULL	ACG / Δ-lifting

Figure 6 shows the morphology taxonomy schematically.

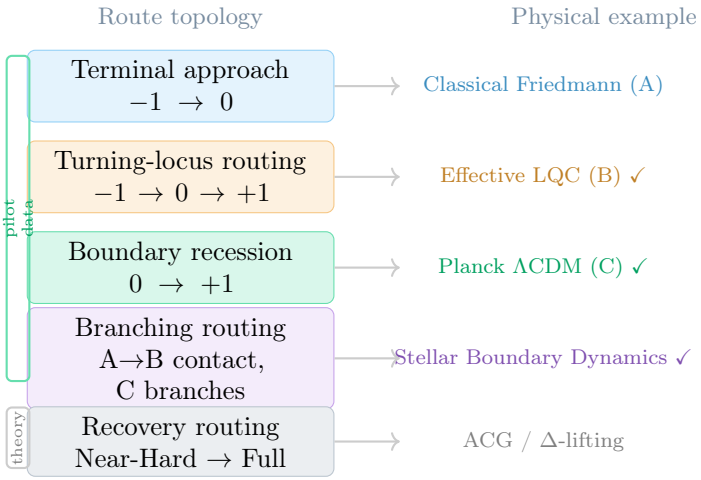

Figure 6: Boundary Routing morphology taxonomy. Modes with ✓ are instantiated in the UNNS pilot corpora. Terminal approach, turning-locus routing, and boundary recession are established in this corpus (A, B, C). Branching routing is established in Stellar Boundary Dynamics I. Recovery routing is theoretically motivated by the ACG framework.

14 Structural Alignment with the UNNS Program

14.1 Margin-Confinement Law

The Margin-Confinement Law [3] establishes that identity-preserving physical trajectories remain confined to $\mathcal{M}_{\text{adm}}$. The cosmological result refines the dynamical picture of confinement. A trajectory may approach a finite critical locus at which a provisional margin coordinate reaches zero without entering $\mathcal{M}_{\text{adm}}^{c}$. Because the route coordinate used here is not yet a canonical metric distance on $\mathcal{M}_{\text{adm}}$ (Open Problem 14.1), the precise statement is: *a finite critical locus associated with the provisional boundary coordinate can realize what operationally appears as turning-locus confinement.* This provides at least two confinement mechanisms:

(i) Barrier confinement: trajectory cannot reach $\partial\mathcal{M}_{\text{adm}}$ and remains interior by margin preservation.

(ii) Turning-locus confinement: trajectory reaches a finite locus, reverses orientation, continuing through a locus admissible under the full-path α test while the associated direct branch encoding remains admissible under STRUC-I and STRUC-PERC-I.

The cosmological corpus is consistent with (ii).

14.2 Percolative Realizability Principle

The PRP [2] establishes admissibility and connectivity as distinct structural coordinates. The pilot corpus demonstrates why three axes are required: the same final percolation class (FULL) coexists with different connectivity depths (κ_{conn} ratio 7.5×), structural pressures ($\bar{\rho}$ ratio 7.4×), and route topologies (three distinct classes). Same class $\not\Rightarrow$ same structural position.

14.3 Canonical metric roadmap

The current route coordinate (cumulative $|\Delta \ln a|$) is path-intrinsic and has not been frozen as a canonical metric distance on $\mathcal{M}_{\text{adm}}$.

Open Problem 14.1 (Canonical Boundary Metric for Cosmological Routing)**.** Construct a metric $d_{\mathcal{M}_{\text{adm}}}(\Gamma(s), \partial\mathcal{M}_{\text{adm}})$ satisfying:

(i) Uses the same formula for A, B, and C;

(ii) Is nonnegative on all represented routes; vanishes only at a verified terminal boundary; remains strictly positive at an admissible turning locus;

(iii) Decreases monotonically along Dataset A;

(iv) Decreases then increases along Dataset B (minimum at the turning locus);

(v) Increases monotonically along Dataset C;

(vi) Distinguishes terminal from turning behavior;

(vii) Remains stable under grid and normalization changes;

(viii) Correlates with structural pressure and α sensitivity.

Until this metric is established, the route coordinate and provisional margin are diagnostic-only. The Local Geometry manuscript [6] establishes the required bi-Lipschitz distance framework; connecting it to the cosmological turning-locus structure is identified as a priority for the extended program.

15 Additional Structural Predictions

Section 12 provides the cross-model taxonomy. Two additional predictions follow from the pilot-corpus result alone.

Singular classical models. A singular classical model without an added continuation mechanism is expected to exhibit represented terminal approach in its classical chart. Its detailed phase-sign vector may depend on matter content and the selected observables; Dataset A supplies one realized signature ($\bar{\mathbf{\Sigma}}_P = (-,+,+,-)$) rather than a universal one. The controlled realization is Dataset A.

Black-hole interiors. If an interior bounce exists under quantum-corrected dynamics, the prediction is analogous to the cosmological case: classical interior $\rightarrow$ terminal approach; quantum-corrected interior $\rightarrow$ turning-locus routing with a near-bounce sensitivity shell. The UNNS route-sign-reversal criterion (Conjecture 9.2) provides the test.

These predictions are falsifiable through application of Bridge v1.1 to trajectories generated by the respective dynamics.

16 Robustness and Falsification

16.1 Proposed robustness tests

(i) **Route-coordinate robustness.** Repeat classification using cumulative $|\Delta \ln a|$ (current), cumulative $|\Delta H|$, cumulative normalized conformal time, and arc length in multichannel state space. The route class should be invariant.

(ii) **Normalization robustness.** Vary Q-percentile (Q80, Q90, Q95) and response cap (3, 5, 7). The turning-locus structure should persist; its disappearance would indicate sensitivity to normalization choices.

(iii) **Grid robustness.** Repeat with $n = 2001$, 4001, 8001 rows. Verify: bounce location, shell symmetry, onset radius, phase means.

(iv) **Channel ablation.** Remove one signed-flow channel at a time ($\Delta \ln a$, density, curvature, margin). This identifies which channels are essential to the route classification.

(v) **Model variant.** Vary the LQC critical density ($\rho_c = 0.35,\ 0.41,\ 0.50\,\rho_{\mathrm{Pl}}$). The turning-locus classification should be stable if it reflects the route topology, not the specific bounce scale.

16.2 Falsification criteria

Turning-locus route classification fails if:

- the exact turning-locus intervals become structurally unstable under any reasonable normalization;
- pre/post signed-flow vectors do not reverse;
- route continuity breaks at the turning point;
- Dataset B collapses into the same class as A or C under a better canonical chart;
- a canonical chart removes the classification distinction while preserving physical content.

Turning-Locus Shielding Hypothesis 9.1 fails if:

- no sensitivity shell appears in a comparable bounce model;
- instability occurs at the exact turning locus;
- shell symmetry disappears under grid or normalization changes;
- the shell pattern fails grid or normalization robustness tests;
- another effective LQC construction shows no shell while still exhibiting a finite turning route.

A model can be a finite turning route without a symmetric sensitivity shell; the shielding hypothesis is not a necessary condition for route classification.

General Boundary Routing theory fails if:

- route topology is a representation artifact only, with distinct charts producing incompatible class assignments;
- structural measures predict nothing beyond the input equations;
- no second bounce model exhibits turning-locus routing.

17 Observational Bridge

17.1 Route-Topology Implications for Cosmological Perturbations

The route-topology classification developed in this manuscript applies to homogeneous background trajectories. It does not by itself determine the evolution of scalar, tensor, or higher-order perturbations. Nevertheless, the three route classes define distinct background conditions under which perturbations must propagate, and therefore motivate testable perturbation-level hypotheses.

Standard LQC perturbation setting. In effective Loop Quantum Cosmology, cosmological perturbations may be evolved across a quantum-corrected background using dressed-metric [10], hybrid-quantization [13], deformed-algebra [14], or related prescriptions. These approaches differ in their effective perturbation equations, vacuum prescriptions, and treatment of the bounce, and do not yield one universal primordial spectrum. A recurring result in several effective LQC studies is that quantum pre-inflationary evolution can modify infrared and intermediate-wavelength modes while ultraviolet modes recover behavior close to the standard inflationary spectrum. Such effects remain model-dependent. The present manuscript does not calculate these spectra. Its contribution is to provide a structural classification of the background route on which perturbations would evolve.

Terminal-approach backgrounds. For a represented terminal-approach route, the background chart ends at a limiting high-curvature regime without a represented continuation. In classical Friedmann contraction, the background quantities diverge as the mathematical singularity is approached, and conventional perturbation evolution cannot be extended through that limit without additional physics. The route-topology interpretation is:

terminal background route

$\Rightarrow$ no background-defined transfer map through the terminal locus is supplied.

This does not imply that every perturbation becomes unstable before the cutoff; it means that the classical background alone does not define a continuation from pre-terminal perturbations to post-terminal observables.

Finite turning-locus backgrounds. For a finite turning-locus route, the background remains finite and continues from contraction into expansion. A perturbation treatment may therefore define a transfer map

$$\mathcal{T}_k : \left(v_k, \partial_\eta v_k\right)_{\mathrm{pre}} \longmapsto \left(v_k, \partial_\eta v_k\right)_{\mathrm{post}}, \tag{13}$$

where v_k denotes an appropriate scalar or tensor mode variable and η is conformal time. The Dataset B background motivates three structural hypotheses, proposed here as Phase 2 targets.

Hypothesis 17.1 (Perturbation Continuation)**.** Because all tested deformations assigned to the two exact bounce-crossing intervals remain admissible, the turning locus is a candidate for coherent perturbation transfer rather than terminal loss of continuation. This must be tested using an explicit perturbation equation and does not follow from background admissibility alone.

Hypothesis 17.2 (Route-Localized Spectral Modification)**.** The symmetric near-bounce sensitivity shells identify the route neighborhood in which perturbation transfer may be most sensitive to background modifications. If a correspondence exists between route position and characteristic comoving scale, deviations from a standard primordial spectrum should be concentrated in a finite scale range associated with the bounce and its

surrounding transition shell. The near-bounce shell motivates testing whether perturbation modifications are localized to scales associated with the transition regime; it does not predict a specific CMB anomaly or low-ℓ suppression value.

Hypothesis 17.3 (Background-Symmetry Transfer Test)**.** The background empirical phase-sign vectors satisfy $\bar{\boldsymbol{\Sigma}}_{P,B,\mathrm{post}} \approx -\bar{\boldsymbol{\Sigma}}_{P,B,\mathrm{pre}}$. Phase-sign reversal provides a background symmetry whose consequences for perturbation transfer remain to be calculated. Scalar, tensor, and entropy modes may respond differently; symmetric background routing need not imply symmetric perturbation transfer.

Boundary-recession backgrounds. A boundary-recession route represents expansion away from an early critical reference regime. Dataset C supplies a Planck-anchored background trajectory but does not independently generate a primordial perturbation spectrum. For models that enter conventional inflationary or radiation-dominated expansion after the bounce, sufficiently short-wavelength modes may lose sensitivity to the earlier critical regime, while longer-wavelength modes may retain pre-bounce or bounce-scale information. Whether this separation occurs and at which scales is a model-dependent question for the perturbation transfer calculation.

Route topology and observable inheritance. The route-topology framework motivates the following provisional classification of backgrounds:

Terminal approach:	no background-defined transfer through the terminal locus,
Finite turning locus:	candidate for modified but continuous transfer,
Boundary recession:	post-critical propagation and late-time observable evolution.

(14)

This classification does not predict a particular CMB anomaly. It identifies which classes permit a well-defined background inheritance map from an earlier route phase into later observables. Background percolation does not establish perturbative stability; scalar and tensor stability must be tested using their own equations.

A completed perturbation-level UNNS analysis must calculate, at minimum, $P_{\mathcal{R}}(k)$, $P_T(k)$, and $r(k) = P_T(k)/P_{\mathcal{R}}(k)$, and where possible higher-order correlation functions. These must then be propagated through a Boltzmann solver and compared with temperature, polarization, lensing, large-scale-structure, and distance data.

Cross-model perturbation expectations. Two cosmologies can share the same turning-locus topology while carrying different observable perturbation inheritances:

$$\Gamma_1 \equiv_{\mathrm{route}} \Gamma_2 \not\Rightarrow P_{\mathcal{R},1}(k) = P_{\mathcal{R},2}(k). \tag{15}$$

Table 12 summarizes the open perturbation questions for the main model families.

17.2 Observational Pipeline and Phase 2 Program

The route-topology classification established in this manuscript operates on background-level trajectories. A full observational program is identified as a Phase 2 target; Figure 7 shows the schematic pipeline.

Table 12: Cross-model perturbation expectations. Background route expectations follow from Table 10; perturbation questions remain open for Phase 2.

Model	Background route	Open perturbation question
Effective LQC	Finite turning locus	Bounce-scale, vacuum, and quantization-prescription dependence
Matter bounce	Finite turning locus	Whether matter contraction generates acceptable scalar spectrum and tensor amplitude
Ekpyrotic bounce	Often asymmetric turning route	Entropy-to-curvature conversion, non-Gaussianity, tensor suppression
Modified-gravity bounce	Model-dependent turning route	Stability of scalar and tensor sectors across correction regime
Cyclic models	Repeated turning loci	Accumulation or resetting of perturbations over successive cycles
Emergent universe	Quasi-stationary corridor → recession	Initial-state selection and transfer out of emergent phase
Conformal cyclic	Possible cross-chart continuation	Definition of perturbation inheritance across conformal identification

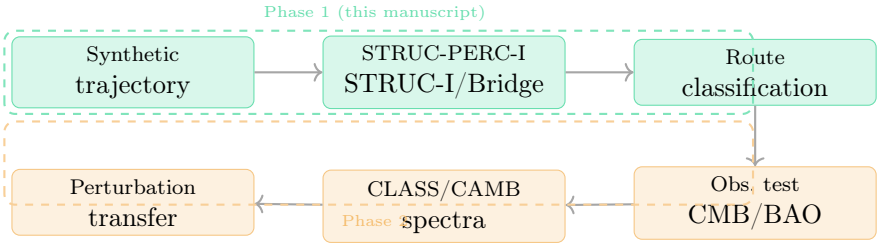

Figure 7: Observational bridge pipeline. Phase 1 (this manuscript, green box): synthetic trajectory construction, structural analysis, route-topology classification. Phase 2 (amber): perturbation transfer to primordial power spectra, comparison with CMB, BAO, Pantheon+ likelihoods, and UNNS re-classification of the observationally constrained model. Phase 2 will test whether route-topology classification is stable under observational constraints from Planck, SDSS/eBOSS, and Pantheon+.

Phase 2 targets include: primordial scalar spectrum n_s, tensor-to-scalar ratio r, low-ℓ CMB features, BAO distances, Pantheon+ distance moduli, and structure growth σ_8. The key question will be whether the LQC trajectory's route-topology classification (turning-locus routing) is stable under observational constraints, or whether constrained versions of the model collapse into different structural regimes.

18 Limitations

Synthetic construction. Datasets A and B are synthetic model trajectories. No claim is made that effective LQC is the correct description of the early universe.

Provisional route coordinate. The shared route coordinate (cumulative $|\Delta \ln a|$) is path-intrinsic and is not a canonical metric distance on $\mathcal{M}_{\text{adm}}$ (Open Problem 14.1).

Provisional margin. The boundary margin used in signed-flow analysis is diagnostic-only. A final canonical UNNS boundary margin for the cosmological setting has not been derived.

Observational validation. Dataset C is anchored to Planck 2018 parameters, but Dataset B's bounce-generated perturbation spectrum has not been tested against CMB, BAO, or Pantheon+ observables.

Single-model scope. The experiment demonstrates the route pattern for one effective LQC construction. Replication across ekpyrotic, modified-gravity, and emergent-universe models is deferred to future work.

19 Conclusion

We have introduced a route-topology layer for cosmological singularity removal and applied it to three matched model trajectories. The central finding is:

Singularity avoidance is not fully characterized by bounded curvature alone. The effective LQC trajectory replaces terminal route topology with admissible turning topology: it reaches a finite turning locus at which all tested α-deformations remain admissible, while the direct post-bounce encoding preserves $A_\kappa = 1$, reverses the empirical phase-sign vector, and continues without structural destruction.

Five structural results support this thesis. All three canonical direct encodings return FULL-percolation. All maintain $A_\kappa = 1$ throughout the tested STRUC-I range. Dataset B is Weak Persistence with mean pressure 7.4× higher than A and C. The full Dataset B path achieves 98.83% α-admissibility persistence with all instability confined to symmetric near-bounce shells and none at the exact turning locus. The orientation-sensitive bridge identifies three distinct route classes (represented terminal approach, finite turning-locus routing, boundary recession). Magnitude-only encoding erases the A–C orientation distinction and cannot identify B's turning topology; B remains magnitude-distinct from A and C through connectivity depth, pressure, and α-response.

The cosmological result extends the Stellar Boundary Dynamics corpus by contributing a second boundary-routing morphology: turning-locus routing alongside the previously established branching routing. Together, the two corpora begin a general taxonomy of how physical systems interact with structural boundaries.

The Turning-Locus Shielding Hypothesis remains open, pending replication across other bounce models and grid refinements. The canonical boundary metric (Open Problem 14.1) and the Phase 2 observational program are identified as priority extensions.

The strongest theoretical claim is the simplest:

> *A structural boundary coordinate can mark admissible route reversal rather than structural destruction. The discriminating test is route-topology class, not coordinate value.*

A Reproducibility: Pipeline and Output Records

A.1 Corpus folder structure

```
cosmological_boundary_routing/
```

```
A_classical_friedmann/canonical/{ladder,struc_perc,alpha}/
B_lqc_bounce/canonical/{ladder,struc_perc,alpha}/
C_planck_lcdm/canonical/{ladder,struc_perc,alpha}/
ABC_bridge/outputs/
tools/
```

A.2 Dataset A

Trajectory: Friedmann, Planck 2018 params, $H < 0$, a=1 $\to 10^{-8}$, 4001 steps in $\ln a$. Direct ladder: sorted $\ln(|H|/H_0)$, 4001 rows. STRUC-PERC-I: FULL, $\kappa_{\text{conn}} = 0.013335$, $n = 4001$, GR = 1.000. α: v2.0.0; $\alpha_{\text{persist}} = 0.99262$.

A.3 Dataset B

Trajectory: eq. (7), $\rho_c = 0.41\rho_{\text{Pl}}$, 2000+1+2000 rows. Direct ladder: post-bounce expansion, sorted $\ln(E_{\text{LQC}})$, 2000 rows. STRUC-PERC-I: FULL, $\kappa_{\text{conn}} = 0.10000$, $n = 2000$, GR = 1.000. α: v2.2.0; signed path; five regions; Q90 normalization; cap 5; $\alpha_{\text{persist}} = 0.98831$.

A.4 Dataset C

Trajectory: Friedmann, Planck 2018 params, $H > 0$, a=$10^{-8} \to 1$, 4001 rows. STRUC-PERC-I and α results: identical to Dataset A under magnitude-only encoding.

A.5 Bridge v1.1 conventions

Route coordinate: cumulative $|\Delta \ln a|$ mapped to $[-1, 0]$ (A), $[-1, +1]$ (B), $[0, +1]$ (C). Normalization: dataset-specific Q90, $f = \Delta/(\text{Q}_{90}(|\Delta|) + |\Delta|)$. Five channels: $\Delta \ln a$, H, density, curvature proxy, margin. Branch-resolved B profile: pre-bounce (1999), turning surface (2), post-bounce (1999) intervals.

A.6 Key archived output files

```
A.../struc_i/chamber_struc_i_v1_0_4_results.json
B.../struc_perc/chamber_struc_i_v1_0_4_results.json
B.../alpha/summaries/B_ALPHA_APPLICATION_SUMMARY_v2_2.csv
B.../alpha/vectors/B_LQC_BOUNCE_5d_vector_v2_2.csv
ABC_bridge/outputs/ABC_orientation_sensitive_bridge_summary_v1_1.csv
ABC_bridge/outputs/ABC_orientation_sensitive_phase_summary_v1_1.csv
ABC_bridge/outputs/ABC_BRIDGE_V1_1_RESULT.txt
```

References

[1] UNNS Substrate Research Program. The Universal Structural Law: Admissibility Bounds on Ordered Physical Systems. *UNNS Working Manuscript*, 2026.

[2] UNNS Substrate Research Program. The Percolative Realizability Principle: Connectivity Margin as a Coordinate of Realizability Space. *UNNS Working Manuscript*, 2026.

[3] UNNS Substrate Research Program. The Margin-Confinement Law: Structural Non-Crossability in Admissibility Space. *UNNS Working Manuscript*, 2026.

[4] UNNS Substrate Research Program. Admissible Cluster Geometry: Recoverable Connectivity in Realizability Space. *UNNS Working Manuscript*, 2026.

[5] UNNS Substrate Research Program. Stellar Boundary Dynamics: Catastrophic Transition as Routing Between Admissible Structural Regimes. *UNNS Working Manuscript*, 2026.

[6] UNNS Substrate Research Program. Local Geometry of Realizability Boundaries: Bi-Lipschitz Distance Representation. *UNNS Working Manuscript*, 2026.

[7] UNNS Substrate Research Program. Bounded Structural Rigidity and Representation-Driven Structure. *UNNS Working Manuscript*, 2026.

[8] M. Bojowald. Loop quantum cosmology. *Living Reviews in Relativity*, **8**(1):11, 2005.

[9] A. Ashtekar, T. Pawlowski, and P. Singh. Quantum nature of the Big Bang: Improved dynamics. *Physical Review D*, **74**(8):084003, 2006.

[10] I. Agullo, A. Ashtekar, and W. Nelson. A quantum gravity extension of the inflationary scenario. *Physical Review Letters*, **109**:251301, 2012. See also: I. Agullo and P. Singh (eds.), *Loop Quantum Cosmology*: A status report. In: A. Ashtekar and J. Pullin (eds.), *Loop Quantum Gravity: The First 30 Years*. World Scientific, 2017, pp. 183–240.

[11] A. Ashtekar and P. Singh. Loop quantum cosmology: A status report. *Classical and Quantum Gravity*, **28**(21):213001, 2011.

[12] P. Diener, B. Gupt, and P. Singh. Chimera: A hybrid approach to numerical loop quantum cosmology. *Classical and Quantum Gravity*, **31**(10):105015, 2014.

[13] M. Fernández-Méndez, G. A. Mena Marugán, and J. Olmedo. Hybrid quantization of an inflationary universe. *Physical Review D*, **86**(2):024003, 2012.

[14] T. Cailleteau, J. Mielczarek, A. Barrau, and J. Grain. Anomaly-free perturbations with inverse-volume and holonomy corrections in Loop Quantum Cosmology. *Classical and Quantum Gravity*, **29**(9):095010, 2012.

[15] R. Brandenberger and P. Peter. Bouncing cosmologies: Progress and problems. *Foundations of Physics*, **47**(6):797–850, 2017.

[16] J.-L. Lehners. Ekpyrotic and cyclic cosmology. *Physics Reports*, **465**(6):223–263, 2008.

[17] Planck Collaboration. Planck 2018 results. VI. Cosmological parameters. *Astronomy & Astrophysics*, **641**:A6, 2020.

[18] R. Penrose. *Cycles of Time: An Extraordinary New View of the Universe*. Bodley Head, London, 2010.

UNNS Substrate Research Program · unns.tech · 2026
Companion: USL · PRP · MCL · ACG · Stellar Boundary Dynamics I · LG · RDS
Instruments: STRUC-PERC-I v2.5.0 · STRUC-I v1.0.4 · Bridge v1.1 · α-Deformation v2.0/v2.2